US010587026B2

(12) United States Patent
Holloway et al.

(10) Patent No.: US 10,587,026 B2
(45) Date of Patent: Mar. 10, 2020

(54) **FULLY INTEGRATED BROADBAND INTERCONNECT**

(71) Applicant: **The Government of the United States of America, as represented by the Secretary of the Navy**, Arlington, VA (US)

(72) Inventors: **Jack W. Holloway**, Arlington, VA (US); **Ruonan Han**, Winchester, MA (US)

(73) Assignee: **The Government of the United States of America, as represented by the Secretary of the Navy**, Washington, DC (US)

(*) Notice: Subject to any disclaimer, the term of this patent is extended or adjusted under 35 U.S.C. 154(b) by 102 days.

(21) Appl. No.: **15/882,771**

(22) Filed: **Jan. 29, 2018**

(65) **Prior Publication Data**

US 2018/0219270 A1 Aug. 2, 2018

Related U.S. Application Data

(60) Provisional application No. 62/451,398, filed on Jan. 27, 2017.

(51) **Int. Cl.**
H01P 5/08 (2006.01)
H01P 5/02 (2006.01)
(Continued)

(52) **U.S. Cl.**
CPC ***H01P 5/087*** (2013.01); ***H01L 23/15*** (2013.01); ***H01L 23/5226*** (2013.01);
(Continued)

(58) **Field of Classification Search**
CPC . H01P 5/028; H01P 5/087; H01P 3/16; H01L 23/15; H01L 23/53257; H01L 23/5226; H01Q 13/22
(Continued)

(56) **References Cited**

U.S. PATENT DOCUMENTS

2002/0021197 A1* 2/2002 Elco H01P 1/16 333/248
2010/0328188 A1* 12/2010 Chang H01Q 21/064 343/893

OTHER PUBLICATIONS

W. Liu et al., "Exploration of electrical and novel optical chip-to-chip interconnects," IEEE Des. Test., vol. 31, No. 5, pp. 28-35, Oct. 2014.

(Continued)

Primary Examiner — Robert J Pascal
Assistant Examiner — Jorge L Salazar, Jr.
(74) *Attorney, Agent, or Firm* — US Naval Research Laboratory; Roy Roberts

(57) **ABSTRACT**

Embodiments herein relate to a fully integrated broadband interconnect. The system comprises a first integrated circuit, a second integrated circuit, and a coupler structure to connect the first and second integrated circuits, where the coupler structure includes a base portion and a top portion that are connected by two vertical walls. The top portion has a gap that increases a strength of a transverse electric field across the gap when the coupler structure is operating in an odd higher order mode that is horizontally polarized, where the coupler structure is full of a dielectric material, and where the cross-sectional width of the coupler structure is tapered in a direction of wave propagation. The system further comprises a dielectric waveguide attached to the top portion of the coupler structure, where the dielectric waveguide supports the odd higher order mode and an even higher order mode.

11 Claims, 6 Drawing Sheets

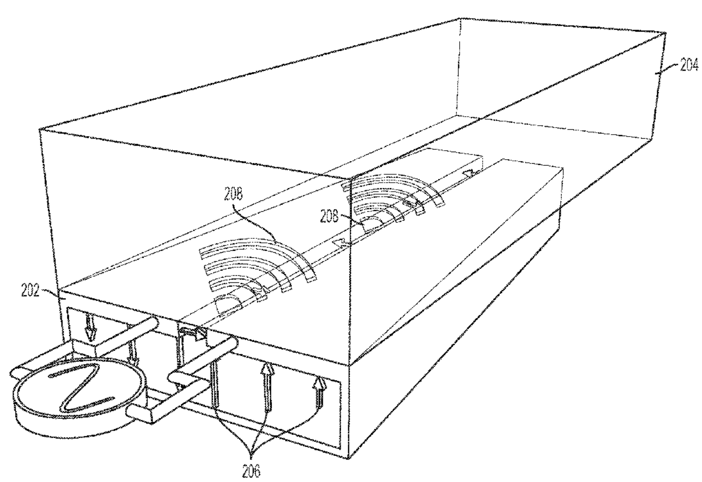

(51) **Int. Cl.**
H01P 3/16 (2006.01)
H01L 23/15 (2006.01)
H01L 23/532 (2006.01)
H01L 23/522 (2006.01)
H01Q 13/22 (2006.01)

(52) **U.S. Cl.**
CPC ***H01L 23/53257*** (2013.01); ***H01P 3/16*** (2013.01); ***H01P 5/028*** (2013.01); *H01Q 13/22* (2013.01)

(58) **Field of Classification Search**
USPC .... 333/22 R, 81 B, 157, 208, 211, 239, 248, 333/254, 255, 21 A
See application file for complete search history.

(56) **References Cited**

OTHER PUBLICATIONS

V. Kumar, R. Bashirullah, and A. Naeemi, "Modeling, optimization and benchmarking of chip-to-chip electrical interconnects with low loss air-clad dielectrics," in Proc. IEEE 61st Electron. Compon. Technol. Conf. (ECTC), May 2011, pp. 2084-2090.
Q. J. Gu, "THz interconnect: The last centimeter communication," IEEE Commun. Mag., vol. 53, No. 4, pp. 206-215, Apr. 2015.
A. E.-J. Lim et al., "Review of silicon photonics foundry efforts," IEEE J. Sel. Topics Quantum Electron., vol. 20, No. 4, Jul./Aug. 2014.
J. S. Orcutt and R. J. Ram, "Photonic device layout within the foundry CMOS design environment," IEEE Photon. Technol. Lett., vol. 22, No. 8, pp. 544-546, Apr. 15, 2010.
J. Michel and L. C. Kimerling, "Electronics and photonics: Convergence on a silicon platform," in Proc. 33rd Eur. Conf. Ehxibit. Opt. Commun. (ECOC), Sep. 2007, pp. 1-2.
D. J. Shin et al., "Integration of silicon photonics into DRAM process," in Proc. Opt. Fiber Commun. Conf. Expo. Nat. Fiber Opt. Eng. Conf. (OFC/NFOEC), Mar. 2013, pp. 1-3.
C. Sun et al., "A monolithically-integrated chip-to-chip optical link in bulk CMOS," IEEE J. Solid-State Circuits, vol. 50, No. 4, pp. 828-844, Apr. 2015.
A. Arbabian, N. Dolatsha, and N. Saiz, "Fully packaged millimetre-wave dielectric waveguide with multimodal excitation," IEEE Electron. Lett., vol. 51, No. 17, pp. 1339-1341, Aug. 2015.
W. Volkaerts, N. Van Thienen, and P. Reynaert, "An FSK plastic waveguide communication link in 40 nm CMOS," in IEEE Int. Solid-State Circuits Conf. (ISSCC) Dig. Tech. Papers, Feb. 2015, pp. 1-3.
A. Hajimiri, "mm-Wave silicon ICs: Challenges and opportunities," in Proc. IEEE Custom Integr. Circuits Conf. (CICC), Sep. 2007, pp. 741-747.
E. Afshari and R. Han, "Progress towards mW-power generation in CMOS THz signal sources," in Proc. Eur. Microw. Integr. Circuits Conf. (EuMIC), Oct. 2013, pp. 117-120.
C. Jiang, A. Cathelin, and E. Afshari, "An efficient 210 GHz compact harmonic oscillator with 1.4 dBm peak output power and 10.6% tuning range in 130 nm BiCMOS," in Proc. IEEE Radio Freq. Integr. Circuits Symp. (RFIC), May 2016, pp. 194-197.
J.-D. Park and A. M. Niknejad, "Y-band on-chip dual half-width leakywave antenna in a nanoscale CMOS process," IEEE Antennas Wireless Propag. Lett., vol. 12, pp. 1476-1479, 2013.
N. Marcuvitz, Waveguide Handbook, Chapter 8: Composite Structures. New York, NY, USA: Dover, 1965.
E. A. J. Marcatili, "Dielectric rectangular waveguide and directional coupler for integrated optics," Bell Syst. Tech. J., vol. 48, No. 7, pp. 2071-2102, Sep. 1969.

* cited by examiner

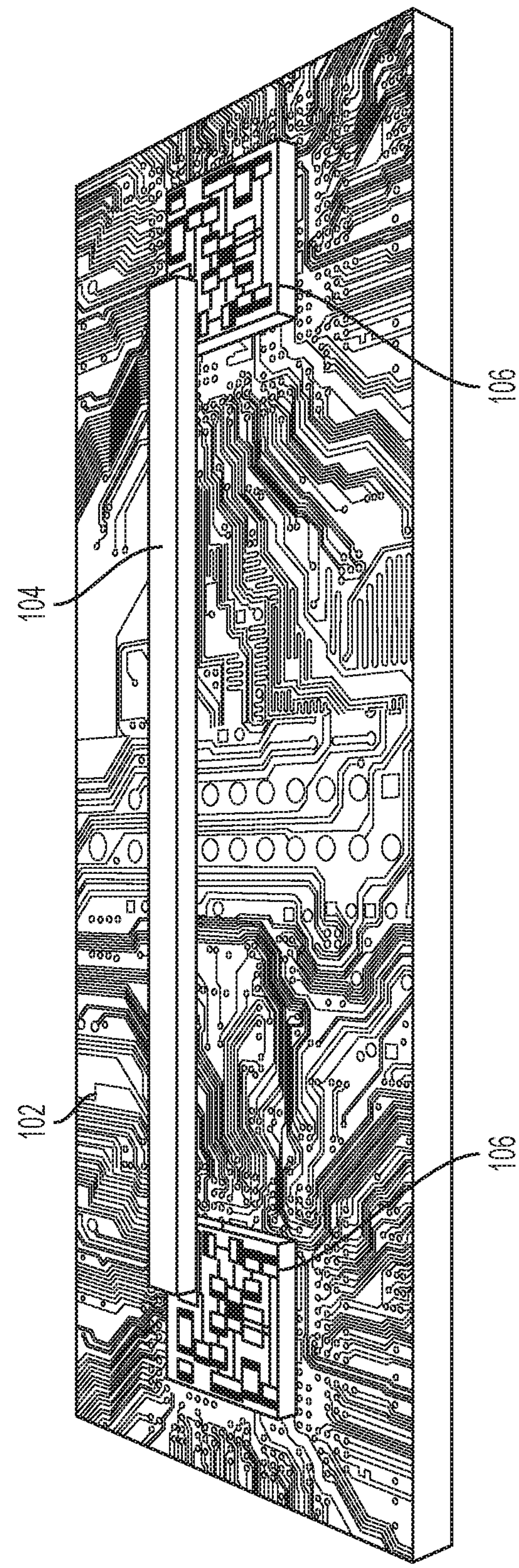

FIG. 1

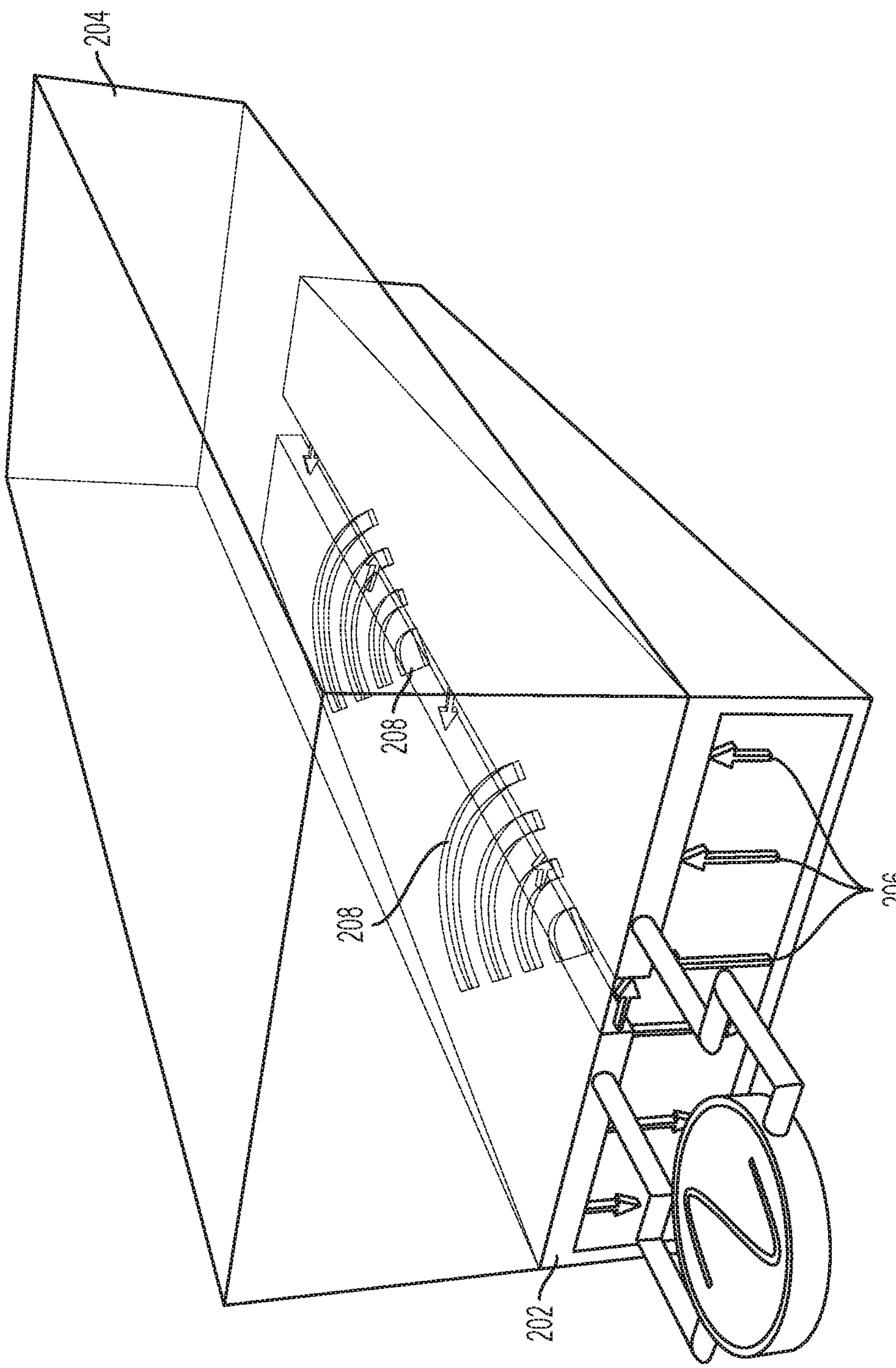

FIG. 2

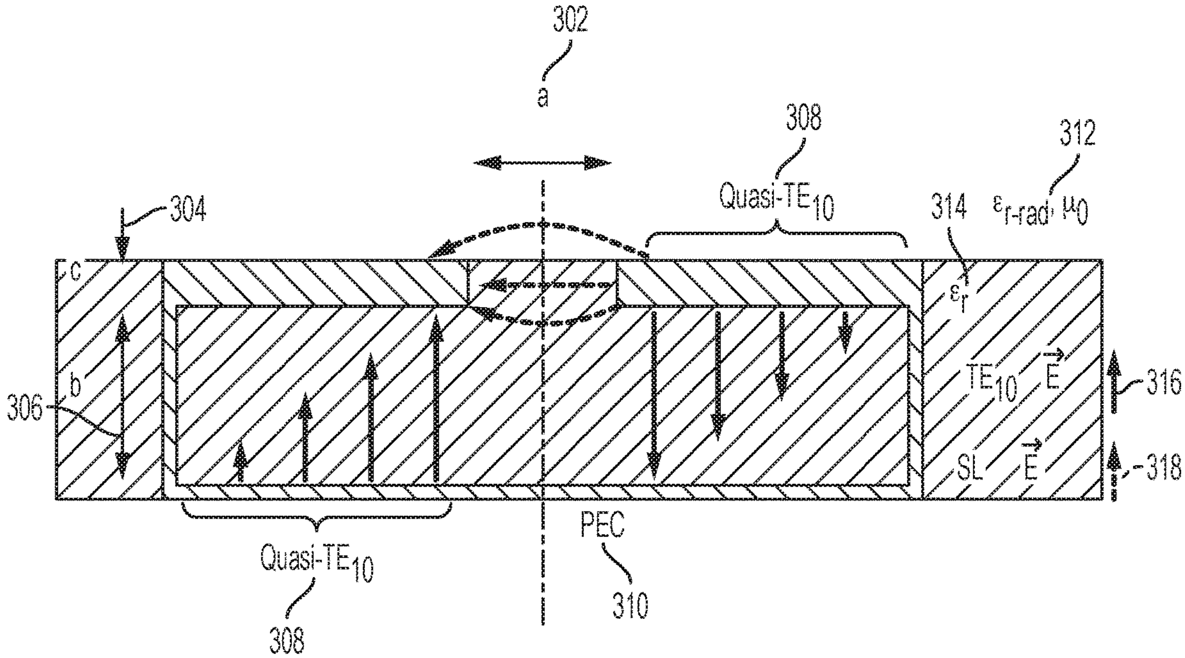
302
a
308
Quasi-TE10
312
314
εr-rad, μ0
304
c
εr
TE10 E
316
306
b
SL E
318
PEC
Quasi-TE10
308
310

FIG. 3A

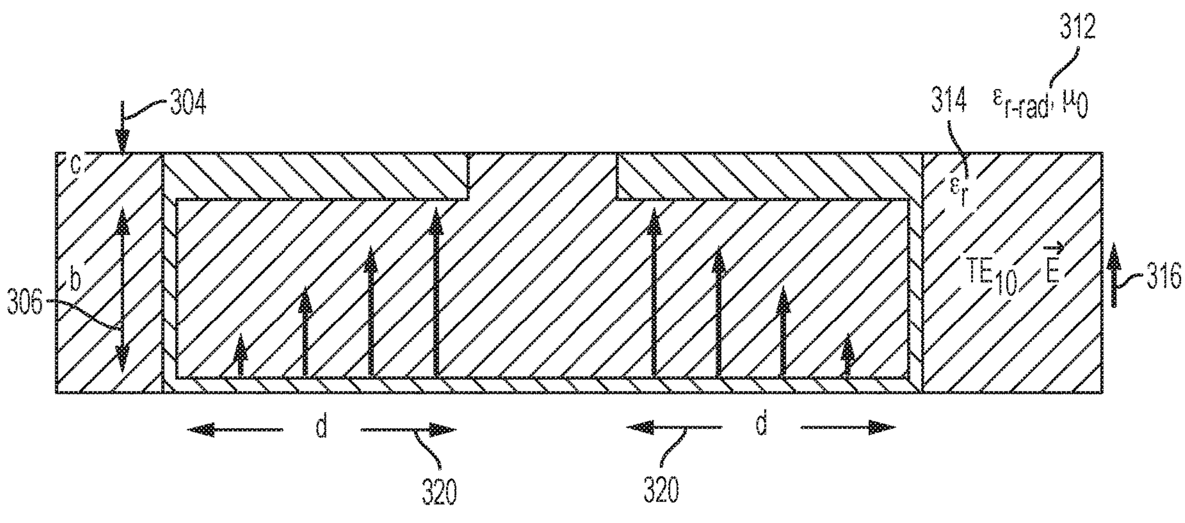
312
314
εr-rad, μ0
304
c
εr
306
b
TE10 E
316
d
d
320
320

FIG. 3B

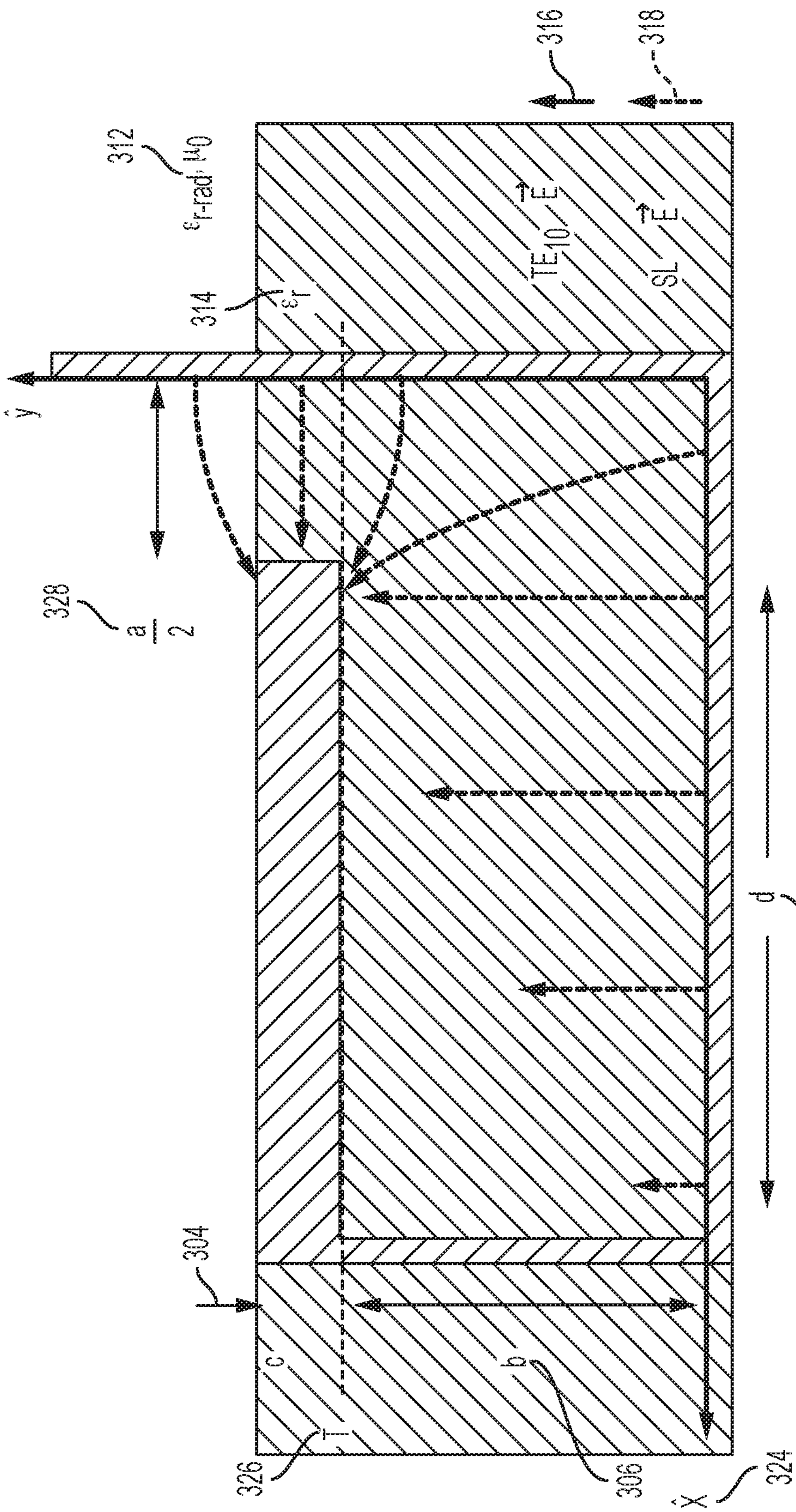
316
318
312
$\epsilon_{r\text{-}rad}, \mu_0$
$TE_{10}\ \vec{E}$
$SL\ \vec{E}$
314
ϵ_r
322
$\hat{y}$
328
$\frac{a}{2}$
d
320
304
c
b
T
326
306
$\hat{x}$
324

FIG. 3C

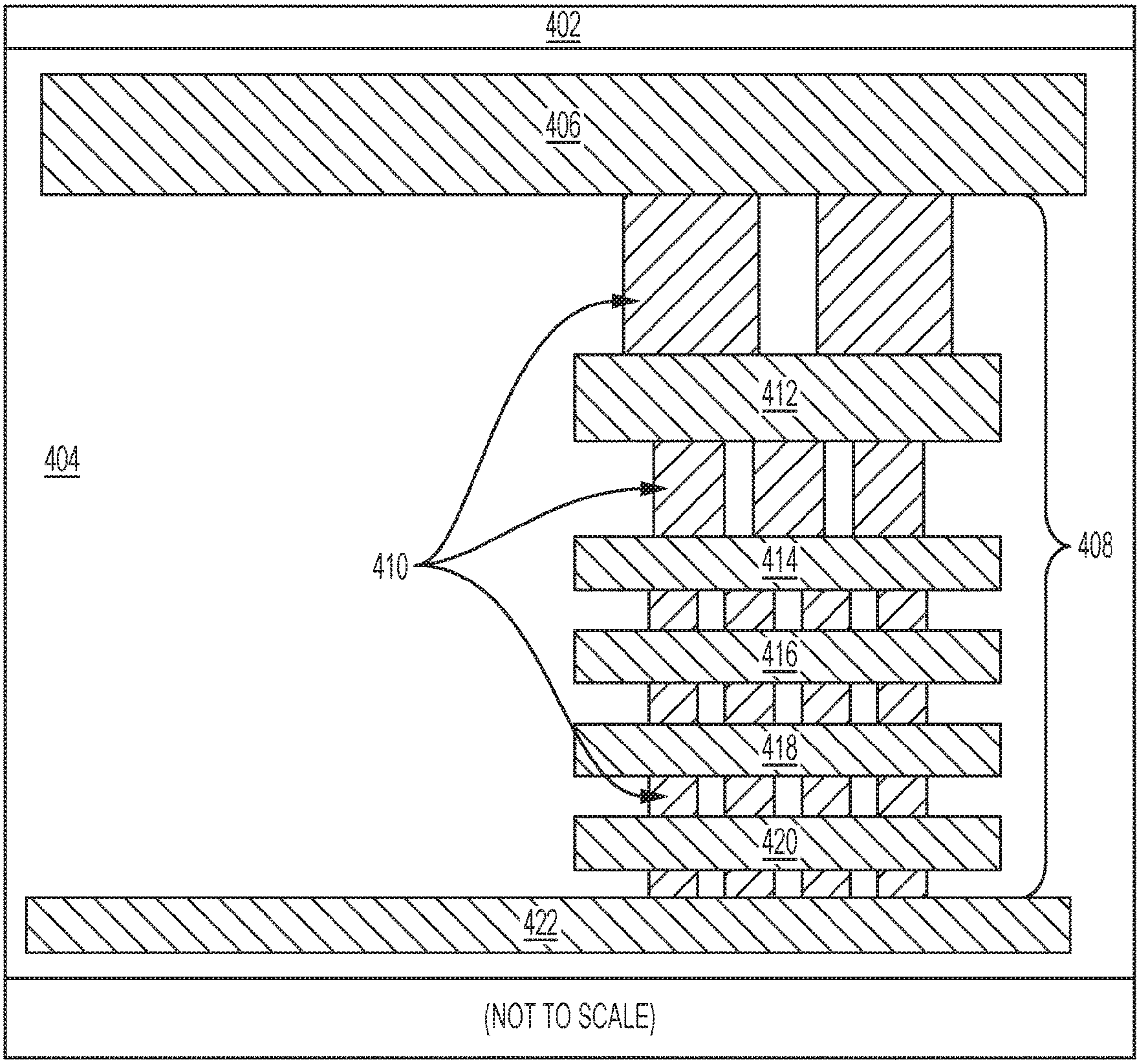

FIG. 4

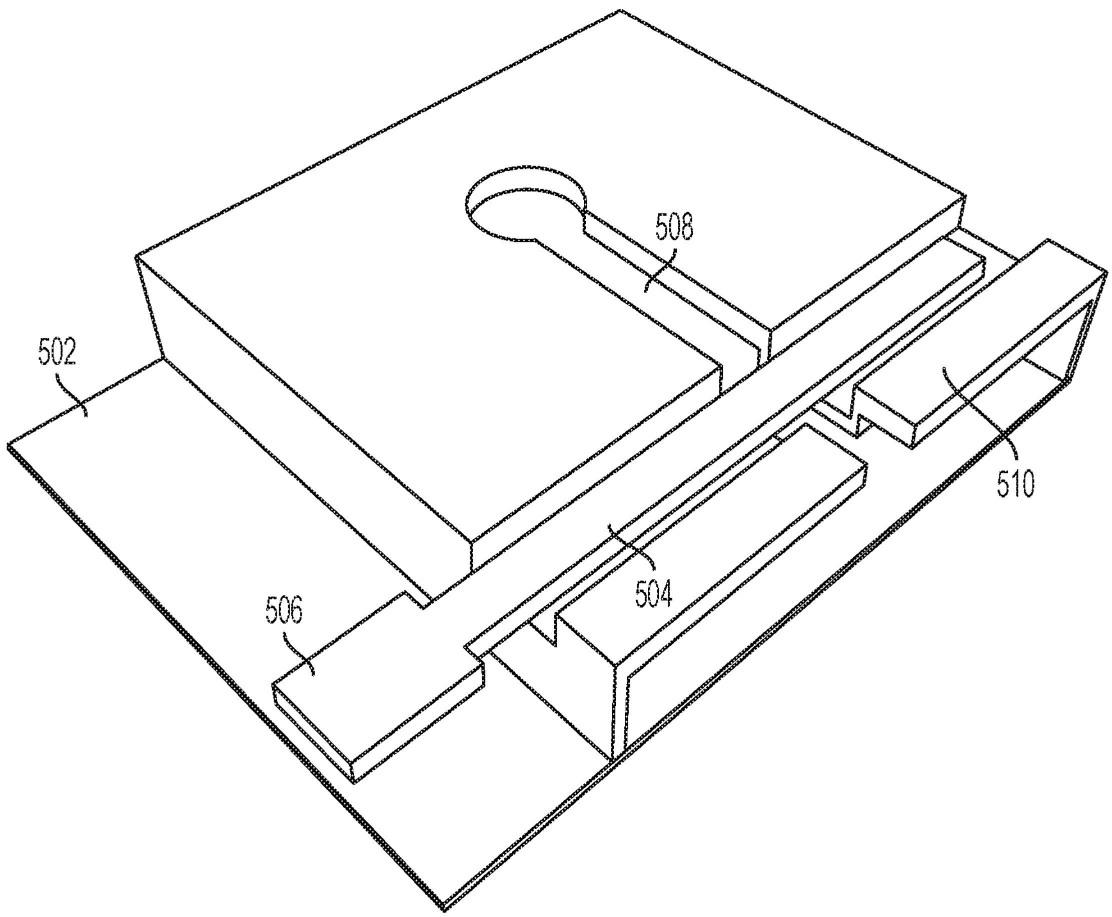

FIG. 5

FULLY INTEGRATED BROADBAND INTERCONNECT

CROSS-REFERENCE TO RELATED APPLICATIONS

This Application is a non-provisional application claiming priority to provisional application 62/451,398 filed on Jan. 27, 2017, under 35 USC 119(e). The entire disclosure of the provisional application is incorporated herein by reference.

BACKGROUND

Traditional interchip interconnect technologies, when deployed for terascale data storage and computing, face issues in transfer speed and energy consumption. The excessive ohmic loss and dispersion associated with copper interconnects in high performance electronic systems have led to a number of efforts focusing on characterization of the physical interconnects, high-speed drivers, and channel equalization in an attempt to mitigate these challenges. In addition, solutions to the board-level (i.e., 1-10 cm link length) and back plane-level (i.e., 10-100 cm link length) interconnects have garnered much attention around electro-optical solutions. These solutions suffer from integration issues surrounding laser sources, waveguides, and photonic devices with traditional silicon systems, as well as electrical-optical/optical-electric conversion and waveguide-chip interfacing issues associated with coupling power on- and off-chip.

A number of efforts have focused on all-electronic solutions to the short-range chip-to-chip communication problem, involving coupling a modulated mmWave or sub-mmWave carrier into a dielectric waveguide—so-called "radio over fiber" schemes. These concepts attempt to harness the wider available bandwidths at these higher frequencies, and require on- and off-chip apertures to radiate into polymer or silicon waveguides. These traditional schemes use lower carrier frequencies, leading to lower bandwidth and I/O density. A number of these works are based on off-chip components, which introduce integration challenges and do not readily lend themselves to higher frequency operation.

Techniques utilizing off-chip radiators, aside from increasing system integration complexity, inherently trade the original bandwidth distance constraint of copper interconnects in driving an off-chip coupler. This effect manifests itself as a decrease in coupling efficiency. In the case of a dual band coupler utilizing mode orthogonality, such systems have been demonstrated with a bandwidth of 35 GHz and coupling loss of 5 dB. A number of efforts have utilized die-to-package bond wires or patch antennas as radiators, coupling energy into plastic tube waveguides. For example, a traditional coupler was demonstrated with a bandwidth of 6 GHz and a coupling loss of 6 dB utilizing air core plastic tube waveguides. This approach presents a number of integration challenges in packaging, especially when high-density I/O integration is needed. Lastly, work has been done on utilizing integrated on-chip antennas to couple modulated carriers into waveguides. In another example, a traditional coupler with a bandwidth of 8 GHz was implemented using a micromachined silicon waveguide, exhibiting a coupling loss of 5.8 dB. While these efforts address the need for an on-chip coupler, they suffer from the well-known bandwidth-radiation efficiency tradeoffs associated with on-chip resonant antennas. This approach also requires the waveguide interface itself to be normal to the radiator surface to maximize the coupling efficiency.

SUMMARY

Embodiments herein relate to a fully integrated broadband interconnect. The system comprises a first integrated circuit, a second integrated circuit, and a coupler structure to connect the first and second integrated circuits, where the coupler structure includes a base portion and a top portion that are connected by two vertical walls. The top portion has a gap that increases a strength of a transverse electric field across the gap when the coupler structure is operating in an odd higher order mode that is horizontally polarized, where the coupler structure is full of a dielectric material, and where the cross-sectional width of the coupler structure is tapered in a direction of wave propagation. The system further comprises a dielectric waveguide attached to the top portion of the coupler structure, where the dielectric waveguide supports the odd higher order mode and an even higher order mode.

BRIEF DESCRIPTION OF THE DRAWINGS

FIG. **1** shows an example fully planar chip-waveguide interface;

FIG. **2** shows an example of two half-mode substrate integrated waveguides (SIWs) that are differentially-driven;

FIGS. **3**A and **3**B show example operating modes of a waveguide in accordance with embodiments of the invention;

FIG. **3**C shows an operating mode for a half-structure waveguide;

FIG. **4** is an example schematic for a substrate integrated waveguide structure in accordance with embodiment of the invention; and

FIG. **5** shows an example mode-converter.

DESCRIPTION

Embodiments of the invention uses a link based on the 220-325 GHz dielectric waveguide and a new class of integrated traveling wave coupler. This coupler is based on a differentially driven half-mode substrate integrated waveguide (HMSIW) topology. The embodiments described herein are compatible with existing commercial integrated circuit (IC) processes and require no wafer postprocessing. This coupler lends itself to straightforward planar integration with a simple rectangular dielectric waveguide. The overall system-level integration concept is illustrated in FIG. **1**. The sub-mmWave frequency range provides much higher bandwidth and data rate compared to mmWave approaches. In addition, the smaller wavelengths in the sub-mmWave regime, compared to mmWave frequency ranges, provide smaller waveguide sizes and smaller guide-to-guide pitches, further increasing the density of high-bandwidth links.

The rapid progress of sub-mmWave and THz signal generation and detection in silicon processes has also spurred interest in modulated sub-mmWave and THz waves for wireline communication. Power generation at these frequencies in silicon typically relies on the use of nonlinearities to produce harmonics, from which the appropriate frequency component is extracted. A SiGe-based THz harmonic oscillator can be implemented with a dc-to-THz conversion efficiency of 2.4%. With increasing silicon device cutoff frequencies, the use of fundamental-mode power generation is an attractive potential, with subsequent improvements in dc-to-THz conversion efficiency. Additionally, receivers in silicon have been demonstrated with sensitivity as low as 29 pW/$\sqrt{\text{Hz}}$. Assuming a nominal detector noise equivalent power (NEP) with an additive white Gaussian noise (AWGN) channel, available bandwidth of 50 GHz, channel and coupler loss of approximately 20 dB, and dc-to-THz conversion efficiencies reported in the literature, embodiments of the invention can theoretically achieve a link efficiency better than 1 pJ/b. The use of coherent detection may further improve the efficiency of such a link. These link efficiency figures make this technology attractive for terascale links with high-density integration.

FIG. **1** shows an example fully planar chip-waveguide interface. Specifically, FIG. **1** shows a printed circuit board (PCB) **102** with two chips **106** that are connected via a dielectric waveguide **104**. The dielectric waveguide **104** supports two quasi-transverse-electric modes and is described in more detail below with respect to FIG. **2**. Embodiments of the invention use a modified leaky wave antenna (LWA) structure in which a coupler cross section is tapered to capitalize on the traveling wave structure's inherent bandwidth while decreasing the required structure length.

FIG. **2** shows an example of two half-mode SIWs that are differentially-driven. Specifically, FIG. **2** shows a coupler structure **202** connected to a dielectric waveguide **204** with the confined electric field **206** and leaky radiation **208** of the coupler structure **202**. When fully implemented in a silicon chip, the coupler structure **202** requires neither wafer post-processing nor off-chip radiators and allows for a low-cost and readily integrated solution for high-bandwidth short range chip-to-chip communication. In some embodiments, the coupler structure **202** is measured with more than 50 GHz of bandwidth, a coupling loss of 4.8 dB, and flat dispersion across the frequency band of 220-270 GHz.

Single-sided HM-SIW antennas are traveling wave radiators that support the first microstrip higher order mode (generally referred to as the EH1 mode). Constant-cross-sectional variants have been integrated on chip, and their single- and differentially-driven variants have been used in arrays. In some of these variants, it is shown that the frequency at which a mode is said to be in the leaky wave region, which can be defined as:

$$\alpha<\beta<k_0\sqrt{\epsilon_r\text{-rad}} \tag{1}$$

and decreased if the structure is excited by the odd EH_1 mode, where k_0 is the free space wavenumber. The longitudinal wave number can be defined as:

$$k_z=\beta-j\alpha \tag{2}$$

and the dielectric constant of the material where the leaky wave power radiates is denoted by ϵ_r-rad **312** as shown in FIG. **3**A. In this example, β is the propagation constant and α is the corresponding attenuation constant of a time-harmonic mode.

Consider a constant cross-sectional coupler structure **202** as illustrated in FIGS. **3**A-**3**B. The inner dimension of the full HM-SIW width can be denoted as 2d+a , with the inner height dimension b **306**, the slot width a **302**, and the top conductor thickness c **304**. The HM-SIW coupler shown in FIGS. **3**A and **3**B is filled with a material with dielectric constant ϵ_r **314**. The entire structure couples to an infinite half-space with dielectric constant ϵ_r-rad **312**.

The HM-SIW coupler structure supports both odd and even EH_1 modes, which are respectively shown in FIGS. **3**A and **3**B. When supporting the odd EH_1 mode as shown by the solid **316** and dashed red arrows **318** in FIG. **3**A, the frequency at which leaky-wave behavior begins for a given structure width is decreased over that of a half-mode LWA or the same structure excited by the even EH_1 mode shown in FIG. **3**B. In addition, using the odd EH_1 mode of FIG. **3**A increases the power radiated due to leaky radiation (described by the attenuate constant α) at a given frequency over the even EH_1 mode of FIG. **3**B or a traditional half-mode LWA. By utilizing the odd EH_1 mode of FIG. **3**A for a given cross section, the amount of energy coupled into a space-leaky mode can be enhanced and the overall required radiator length decreased while maintaining coupling efficiency compared with a structure excited by the even EH_1 mode of FIG. **3**B or a half-mode LWA supporting a TE_{10} mode.

When excited with the odd EH_1 mode, a portion of the electric field contained within the structure and far from the central slot resembles half of a TE_{10} rectangular waveguide mode. In the following discussion, this portion of the mode is referred to as the quasi-TE_{10} **308** portion, and this portion of the field is denoted by the solid red lines **316** in FIG. **3**A. Near the center slot, the increased electric field strength across the gap causes the electric field lines from the top conductor near the gap to terminate, not vertically onto the bottom conductor, but rather on the top conductor on the opposite side of the gap. These fields are similar to a conductor-backed slot-line mode. This portion of the mode is denoted by the dashed electric field lines **318**.

It should be noted that, for a given guide width 2d+a, which is approximated by 2d, at frequencies above:

$$f_{TE}\approx\frac{c_0\sqrt{e_r}}{4d} \tag{3}$$

where c_0 is the free-space speed of light, the energy in the quasi-TE_{10} **308** field is well-confined in those rectangular waveguide regimes on the structure to the left and right of the center slot. As the wavelength of the supported mode is increased, each rectangular guide section of length d **320** can no longer fully support a quarter wave, and some portion of this energy is coupled into the electric field supported between the center slot and the bottom conductor. This portion of the mode is shown by the slot-line fields denoted by the dashed field lines **318** in FIG. **3**A. Once this energy has been coupled into this regime, it will radiate away from the structure in a space leaky mode if the mode's propagation constant satisfies equation (1). In the slot and near field, this coupler structure produces an electric field in which the major component is aligned horizontally, which is matched with the desired horizontally polarized mode in the dielectric waveguide. The similarity between the desired waveguide mode and coupler radiative modes aides in energy coupling. This is in contrast with the field distribution created by a traditional patch antenna. The fringe fields at the edge of a patch form horizontally polarized electric fields in the far field, but the near-field modes have much more structure. Traditional patch antennas exhibit larger near-field electric field intensity at the edge with smaller field intensity in the center of the patch. The dissimilarity, in the near field, of this mode and the desired waveguide mode does not encourage energy coupling from the radiative mode into the waveguide mode.

By decreasing the structure width, 2d, longitudinally as shown in FIG. **2**, such a coupler structure **202** produces regions in which energy in a previously propagating quasi-

TE_{10} portion of the mode impinges on a narrower cross section where that energy couples into the field supported across the center gap. By virtue of the differential excitation (the odd EH_1 mode shown in FIG. 3A), this same structure facilitates the lower frequency onset of space-leakage, as defined in (1), and simultaneously increases the rate of leakage a over the leaky regime. In this way, this coupler structure **202** is able to radiate with the same efficiency while requiring less length.

The coupler structure **202** provides a number of advantages over traditional on-chip antennas:

1. Its enclosed nature provides mode confinement away from the bulk silicon, thus decreasing unwanted energy coupling into the substrate.
2. The coupler structure **202** is a traveling wave structure leading to a wider bandwidth than in resonant structures.
3. The coupler near-field mode is structurally similar to the desired mode of the dielectric waveguide, improving coupling efficiency.

Structures similar to the coupler structure shown in FIG. **3**C have been studied using modal analysis that assumed a zero-thickness top conductor. In contrast, the coupler structure described herein makes use of a thick top metal of thickness c **304**. The conductor-backed slot-line and its odd hybrid mode behavior have also been modeled, utilizing both modal analysis and circuit approximations; however, this analysis does not support modes constrained laterally in the bottom portion of the structure. In contrast, the operation of the coupler structure of FIGS. **3**A and **3**B relies on the vertical SIW walls to contain energy that might otherwise be dissipated into bulk silicon surface waves. In a comparison with full-wave analysis, both of the aforementioned analyses were found to deviate significantly.

An analytical model of the relationship of the odd EH_1 mode longitudinal propagation constant, k_z, as a function of guide dimensions provides insight into the space leaky wave behavior, or the propagation constant β to be specific, as the cross section of the structure is modified. With respect to FIGS. **3**A and **3**B, it can be assumed that the conductors (physically realized by aluminum metallization and arrays of tungsten vias) are perfect electric conductors (PECs) **310**. Further, the electric field distribution of the odd EH_1 mode shown in FIG. **3**A is differentially symmetric, and thus its transverse equivalent network can be represented by a half structure utilizing a PEC boundary condition such as the one shown in FIG. **3**C.

The geometry in FIG. **3**C can be analyzed by a closed-form transverse resonance expression. The resonance condition plane T **326**, denoted by the dashed horizontal line, provides a convenient reference with which to categorize the energy stored in various portions of the fringe fields near the center gap.

Susceptances account for stored energy in the main guide (below the resonance plane T **326**) underneath the slot. Above the resonance plane T **326**, it is assumed that the gap **328** is narrow enough such that only a transverse electric field is supported across the gap **328**. In the gap **328** between the top conductors, from T **326** to the $\epsilon_r - \epsilon_{r-rad}$ dielectric interface, a horizontally polarized TE_{10} mode (that is $E_x \neq 0$, $E_y = E_z = 0$), is supported in the vertical $\hat{y}$ direction **322**. The equivalent susceptances of the energy stores in the field directly above T are written as:

$$\frac{B_s}{Y_0} = \frac{4b}{\lambda_g} \ln \csc \frac{\pi a}{2b} \tag{4}$$

where the guide wavelength is:

$$\lambda_g = \frac{\lambda_0}{\sqrt{e_r - \left(\frac{\lambda_0}{4d}\right)^2}}. \tag{5}$$

The coupling coefficient, modeled by a hypothetical transformer in a structure such as shown in FIG. **3**C with a turns ratio of:

$$n_{cs} = n_c \sqrt{\frac{a}{b}} \tag{6}$$

accounts for the difference in the modal voltages in the horizontal portion of the structures and those in the gap **328**. The short section of vertical parallel plate, of length c **304** along $\hat{y}$ **322**, seen from reference plane T **326** and up can be represented as a short transmission line of length c **304**. The admittance looking into this transmission line can be expressed as:

$$\frac{Y_c}{Y_0} = \frac{\frac{Y_r}{Y_0} + j \tan k_y c}{1 + j \frac{Y_C}{Y_0} \tan k_y c}. \tag{7}$$

The equivalent radiation admittance from a rectangular waveguide into a dielectric half-space is:

$$\frac{Y_r}{Y_0} = \frac{G_r + jB_r}{Y_0} = \frac{\sinh\left(\frac{k_y a}{2}\right) + j\sqrt{e_r} \sin A}{\cosh\left(\frac{k_y a}{2}\right) + \cos A} \tag{8}$$

for

$$A = \frac{k_y a}{\pi} \ln\left(\frac{e}{\gamma} \frac{4\pi}{k_y a}\right) - 2 \sum_{n=1}^{\infty} \left[\sin^{-1}\left(\frac{k_y a}{2\pi} \frac{1}{n}\right) - \left(\frac{k_y a}{2\pi} \frac{1}{n}\right)\right] \tag{9}$$

where $\gamma \approx 1.781$ and Napier's constant, e, is 2.718. In addition, it is assumed that a single transverse electric mode above T **326** in FIG. **3**C and single TE mode operation in the horizontal portion of the structure to the left of the gap **328**. As this entire region is filled with the same dielectric, k_x is assumed below the reference plane T **326** and away from the slot is equal to k_y above T **326**.

In order for a transverse resonance to occur, Y_{up} and Y_{down} phases at the resonance plane should cancel, which can be solved for the transverse wavenumber in the horizontal portion of the coupler structure away from the slot as:

$$k_x = \sqrt{k_0^2 \epsilon_r - k_z^2} \tag{10}$$

which in turn yields the longitudinal wavenumber, k_z, and subsequently, the propagation β and attenuation α constants.

In comparison to the case of an untapered structure, the tapered structure **202** shown in FIG. **2** provides a progressively higher cutoff frequency as the wave **206** travels longitudinally down the structure. In addition, the traveling wave **206** also exhibits a commensurate increase in the rate of leakage α in the leaky regime. While an untapered structure will leak energy into the covering semi-infinite dielectric, the length required to achieve high levels of coupling is much longer. In this manner, the tapered structure **202** is capable of forcing energy otherwise confined in a quasi-rectangular waveguide mode into a space leaky wave mode in a longitudinally shorter aperture while maintaining a large bandwidth.

It has been shown that the described dielectric **204** into which the leaky wave **208** propagates is compatible with the Rogers Corporation R3006 type laminate dielectric (ϵ_r–rad=6.15). Embodiments of the invention have a desired operating range of 220-320 GHz, the total guide **204** width ranges from approximately 300-400, μm to provide leaky operation across the entire band, while maximizing leakage, α **208**, for a given length. These values can be utilized in a full-wave optimization as a starting point to co-optimize the dielectric waveguide cross section **204** and the coupler **202** geometry to minimize insertion loss and coupler return loss.

In some embodiments, the waveguide **204** supports two quasi-transverse-electric modes, the E_{mn}^x and E_{mn}^y modes, in which the bulk of the field is polarized in either the $\hat{x}$ or $\hat{y}$ direction, respectively. The dispersion relationship can be described as:

$$k_z=\beta=\sqrt{\epsilon_{r1}k_0^2-k_x^2-k_y^2}, \tag{11}$$

which can be used to determine the cutoff frequencies of a given mode. During initial testing, a test waveguide with a height of approximately 250 μm, a width of approximately 400 μm, and a length of approximately 500 μm was used. In this example, Marcatili's approximation are used to provide a reasonable starting point for full-wave electromagnetic simulation from which optimization is used to converge to a guide cross section that is mode-matched to the tapered coupler structure, maximizing power transfer as described below.

Using the coupler dimensions and the waveguide cross section derived as described above, the coupler and waveguide dimensions ($L_{coupler}$, a, and a+2d_w and a+2d_n at the coupler's wide and narrow widths, respectively) can be designed in the IHP SG13G2 SiGe BiCMOS BEOL process and optimized with the aid of full-wave simulation tools. An example of a designed coupler and waveguide is shown in FIG. **4**. In this example, the coupler has a 3 μm thick top metal **406** with a distance of 9.83 μm between the top of the bottom metal **422** and the bottom of the top metal **406**. The top metal **406** and bottom metal **422** act as horizontal conductors. The vertical walls **408** of the coupler are composed of intermediate metal interconnects **412-420** and arrays of vias **410**.

A simplified model of the structure can be implemented in a commercial full-wave electromagnetic simulation package. In the simplified model, the coupler geometry was excited by a 50Ω source across the structure's slot at the wider end of the coupler as shown in FIG. **2**. Immediately on top of this coupler topology, a rectangular fiber with a thickness, dh, of 250 μm (to account for commercially available material thicknesses) rectangular cross-sectional fiber completely overlays the coupler slot and extends 500 μm beyond the narrow end of the structure. The second port of the model consists of a wave port at the end of this 500 μm protrusion. The coupler structure and waveguide dimensions were optimized with a≈3.5 μm, dw≈180 μm at the widest end of the structure, and dn≈100 μm for the narrowest end of the structure to minimize the structure return and insertion loss across the desired 220-325 GHz operating band. From this point, full-wave simulations were executed to tune the coupler length, $L_{Coupler}$.

For example, a coupler length, $L_{coupler}$, of 750 μm can be chosen for fabrication to maintain an average insertion loss of approximately 4 dB with better than 8 dB of return loss across the band, while minimizing on-chip area.

A mode converter such as the one shown in FIG. **5** can be used to facilitate on-wafer testing of the coupler to provide a broadband conversion of an on-wafer 50Ω microstrip mode to a 50Ω slot-line mode, driving the coupler structure. The microstrip feed line **506** is implemented using the top and bottom metal layers described above with respect to FIG. **4**, with a trace width of 17 μm. In addition, this mode-converter was used to compensate the slightly inductive input reactance of the coupler. By using Top Metal **1 412** under Top Metal **2 406** from FIG. **4** in the mode-converter feed structure **510**, a capacitive waveguide E-plane iris is presented in parallel with the driving point of the coupler input, providing an improved input match. This section of the mode converter presents itself, essentially, as a grounded coplanar **504** waveguide (GCPW) or half of a rectangular coaxial transmission line with a trace width of 4 μm, and a gap width of 20 μm. The distance between the bottom of the signal trace and the GCPW effective ground **502** is 3 μm. The mode converter is approximately a quarter-wave in length at the center of the operating band, comprised of a 170 μm long 3.5 μm wide slot **508** and a 20 μm diameter circular choke for broadband response. This mode converter is designed with the same cross section (width, height, gap width, etc.) as the coupler structure, enabling direct connection to the coupler structure. With the integration of on-chip electronics, this mode-converter may not be necessary, further decreasing the end-to-end insertion loss and reducing the overall coupler size.

On-die calibration standards can be designed and implemented, enabling multiline transmission, reflection, and line (mTRL) calibration. Microstrip lines of lengths commensurate with those driving the coupler and mode-converter structures were available on die to aid in de-embedding the microstrip loss. Lastly, a back-to-back mode-converter was implemented on die to enable de-embedding the response associated with the mode-conversion and subsequent additional dielectric and ohmic losses.

Returning to FIG. **1**, the substrate **102** should be selected in order to minimize evanescent mode coupling into areas surrounding the dielectric waveguide **104**. For example, a low dielectric constant Rogers TMM3 type laminate ceramic composite material (ϵ_r≈3.27) can be used for the substrate **102**. In this example, the substrate material can be laser ablated for individual die position, depressed 300 μm from the material surface. Areas underneath the desired dielectric waveguide routing can be removed to reduce the waveguide's evanescent field interaction with the substrate.

In one example, Rogers R3006 type laminate can be selected as the dielectric waveguide interconnect **104** for its specified dielectric constant, machinability, low loss, and wide availability. These waveguides can be made from bulk 250 μm thick unclad R3006 type laminate that are laser cut to a width, dw, of 400±10 μm. In this example, a number of straight and curved waveguide pieces can be cut to align with the individual die and coupler positions after bonding to the test coupon/substrate described below.

After the individual dies **106** are placed, aligned, and bonded to the substrate material **102**, the dielectric waveguides can then be individually bonded on top of the chips' passivation layers with, for example, EPOTEK 713 type epoxy. In one case, distance between the top of the individual die passivation layer and the bottom of the dielectric waveguide (denoted as ΔH_{gap}) has an effect on the structures ability to phase shift. For example, compared to a 2.0 cm waveguide with bends, a 2.0 cm straight waveguide has an additional measured average insertion loss of 2.5 dB, partly due to the 17.5 μm ΔH_{gap}. A simulated loss increase corresponding to ΔH_{gap} shows a significantly reduced insertion loss and increased phase delay of a 0.1 cm waveguide compared to longer waveguides, indicating that this shorter length is short enough to support energy coupling into not only a traveling wave mode in the dielectric guide but also a radiative mode coupled into the opposite side of the link.

After accounting for the excess coupling loss present in 2.0 cm straight guide sample bonds, the 1.0 and 2.0 cm average losses over the band are currently estimated at only 0.5 dB/cm. Given this waveguide loss, it is estimated that the insertion loss of a single coupler is approximately 4.8 dB, which agrees well with the simulated data of approximately 3.8 dB per transition. The performance of this interchip link system exceeds that of the traditional systems. A comparison of available "radio of fiber" coupler performance is provided below in Table I.

TABLE I

Ref.	Present Invention	Terahertz Interconnect	mm-wave Dielectric Waveguide	mm-wave Link w/ CMOS trans.	Full-duplex Plastic Waveguide
Center Freqs.	275 GHz	195 GHz	77 GHz 75 GHz	60 GHz	57 GHz 80 GHz
BW	50 GHz	8 GHz	35 GHz	6 GHz	6 GHz
Ins. Loss	4.8 dB	5.8 dB	5 dB	6 dB	7 dB (est)
Guide Cross	400 μm	500 μm	850 μm	1.6 mm	1.1 mm
Section	250 μm	300 μm	850 μm	Radius	8 mm
Notes	1	2	3	2	3

1 On-chip coupler with a planar chip-waveguide interface
2 On-chip coupler with the waveguide attached to the chip at 90° angle
3 Off-chip coupler with a planar chip-waveguide interface

Embodiments of the invention provide a fully integrated on-chip traveling wave power coupler, based on a differentially driven HM-SIW structure, co-designed with a low-cost planar rectangular dielectric waveguide. The described structure achieves an insertion loss of 4.8 dB, which is the lowest among all published works in the millimeter-wave frequency band. The increased operating frequency provides the smallest waveguide cross section and the potential for a lower guide-to-guide pitch. A usable bandwidth of 50 GHz was measured during testing, which provides an opportunity for very high data rate transmission. Further, the described structure provides the most straightforward path for on-chip integration. The proposed coupler structure also enables the simplest implementation of a planar interface between the chip and dielectric waveguide. The simple system-level planar integration makes use of low-cost commercially available materials already in widespread use in the printed circuit board (PCB) industry.

The described structure is demonstrated for the first time at these frequencies, providing smaller guide size, lower pitch, and more available bandwidth than demonstrated in traditional system. Lastly, the small differences in losses between the 1.0 and 2.0 cm samples indicates low loss in this guide material at these frequencies, approximately 0.5 dB/cm. This in-guide loss makes this invention viable for link lengths up to approximately one meter.

While the invention has been described with respect to a limited number of embodiments, those skilled in the art, having benefit of this disclosure, will appreciate that other embodiments can be devised which do not depart from the scope of the invention as disclosed herein. Accordingly, the scope of the invention should be limited only by the attached claims.

The invention claimed is:

1. A system comprising:

a first integrated circuit;

a second integrated circuit;

a coupler structure to connect the first and second integrated circuits, the coupler structure including a base portion and a top portion that are connected by two vertical walls,

the top portion having a gap that increases a strength of a transverse electric field across the gap when the coupler structure is operating in an odd higher order mode that is horizontally polarized, wherein the coupler structure is full of a dielectric material, and

wherein a cross-sectional width of the coupler structure is tapered in a direction of wave propagation; and

a dielectric waveguide attached to the top portion of the coupler structure, the dielectric waveguide supporting the odd higher order mode and an even higher order mode.

2. The system of claim **1**, wherein a cutoff frequency for operating the dielectric waveguide in the odd higher order mode is determined according to a dispersion relationship described as:

$$k_z=\beta=\sqrt{\epsilon_{r1}k_0^2-k_x^2-k_y^2}$$

wherein k_z is a longitudinal wavenumber of the coupler structure, $\beta$is a propagation constant, ϵ_{r1} is a dielectric constant of the dielectric waveguide, k_x is a transverse wavenumber in a horizontal portion of the coupler structure, k_0 is a freespace wavenumber, k_y is a transverse wavenumber in a vertical portion of the coupler structure.

3. The system of claim **1**, each of the two vertical walls comprises a plurality of via arrays that are connected by a plurality of intermediate metal interconnects, wherein a height of each of the plurality of via arrays from the top portion to the bottom portion are progressively shorter.

4. The system of claim **3**, wherein the top portion is approximately 3 μm thick, and wherein a distance between a bottom of the top portion and a top of the bottom portion is approximately 9.83 μm.

5. The system of claim **3**, wherein the plurality of intermediate metal interconnects are composed of aluminum and the plurality of via arrays are composed of tungsten.

6. The system of claim **3**, further comprising a mode-converter affixed to a wave generating end of the coupler structure and having a same cross section as the coupler structure, the mode-converter comprising a coplanar waveguide for generating a wave that transmits from the first integrated circuit to the second integrated circuit through the coupler structure, wherein a topmost of said plurality of intermediate metal interconnects is a same metal material as the coplanar waveguide, which presents a capacitive waveguide iris in parallel with a driving point of the coupler structure.

7. The system of claim **6**, wherein the capacitive waveguide iris behaves as a half of a rectangular coaxial transmission line with a trace width of 4 μm, and a gap width of 20 μm.

8. The system of claim **1**, wherein the dielectric waveguide has an operating range of 220-325 GHz.

9. The system of claim **1**, wherein the dielectric waveguide has a width of approximately 300-400 μm.

10. The system of claim **1**, wherein the first and second integrated circuits are affixed to a circuit board that is composed of a ceramic laminate material with a dielectric constant of 3.27.

11. The system of claim **1**, wherein a longitudinal length of the coupler structure is approximate 750 μm.

* * * * *